https://doi.org/10.3311/PPch.44836
Creative Commons Attribution

Periodica Polytechnica Chemical Engineering

GC–MS-Based Untargeted Metabolic Profiling of Oil Palm Stems Associated with *Ganoderma boninense* Infection

Susi Indriani[1*], Adi Pancoro[2], Isdaryanti[3], Andi Besse Poleuleng[1], Sitti Nur Ilmiah[4], Fitri Handayani[5]

[1] Department of Agricultural Production Technology, Agricultural State Polytechnic of Pangkajene Kepulauan, Poros Makassar-parepare Km 83, 90655 Pangkep, Indonesia
[2] Department of Biotechnology, School of Life Science and Technology, Bandung Institute of Technology, Jl. Ganesa 10, 40132 Bandung, Indonesia
[3] Faculty of Teacher Training and Education, West Sulawesi University, Jl. Prof. Dr. Baharuddin Lopa, 91412 Majene, Indonesia
[4] Department of Biology, Faculty of Mathematics and Natural Science, Billfath University, Jl. KH. Abdul Fattah, Lamongan Regency, 62261 Lamongan, Indonesia
[5] Department of Biotechnology, Bacharuddin Jusuf Habibie Institute of Technology, Jl. Balaikota 1, 91125 Parepare, Indonesia
[*] Corresponding author, e-mail: indrianisusi@polipangkep.ac.id

Received: 22 May 2026, Accepted: 17 September 2026, Published online: 10 November 2026

Abstract

Basal stem rot, mainly caused by *Ganoderma boninense*, is a major disease affecting oil palm (*Elaeis guineensis*) and can lead to reduced productivity and plant mortality. This study characterized metabolic changes associated with different levels of *G. boninense* infection in oil palm stem tissue using untargeted gas chromatography–mass spectrometry metabolomics. Stem samples representing healthy, low, moderate, and high infection categories were analyzed, and the resulting metabolic features were processed using multivariate and univariate statistical approaches. A total of 14 features were retained after data processing and filtering. Principal component analysis and partial least squares discriminant analysis showed differences in the overall metabolic profiles among infection categories, while variable importance in projection analysis identified features contributing to group discrimination. However, permutation testing did not provide significant evidence for a classification model beyond chance (ANOVA *p*-value = 0.121), indicating that 121 of 1,000 permuted models achieved an accuracy at least as high as that of the observed model. None of the detected features remained significant after false discovery rate correction. Several fatty acid-related features, including methyl decanoate, methyl myristate, methyl oleate, methyl stearate, and methyl ricinoleate, were prioritized based on their multivariate contribution, abundance patterns, and library-based annotation. These compounds are therefore considered candidate metabolites associated with disease severity rather than validated biomarkers. The findings provide a preliminary view of metabolic variation in oil palm stems associated with *G. boninense* infection and identify candidate features for further validation using larger and independent sample sets.

Keywords

Ganoderma boninense, gas chromatography–mass spectrometry, untargeted metabolomics, oil palm, basal stem rot

1 Introduction

Oil palm (*Elaeis guineensis*) continues to play a central role in agricultural systems across the humid tropics, largely because of its exceptional contribution to the global vegetable oil market, comprising more than 35% of global vegetable oil production [1]. As one of the most productive oil-bearing crops, palm oil accounts for a substantial share of worldwide edible oil output, and its cultivation provides a critical economic foundation for both smallholder households and commercial plantation enterprises in major producing regions [2].

However, the sustainability and productivity of oil palm plantations are severely threatened by basal stem rot (BSR), a progressive disease mainly caused by the soil-borne white-rot fungus *Ganoderma boninense*, which can lead to substantial yield reductions and tree mortality across affected regions [3]. A persistent challenge in managing BSR is the difficulty of early and reliable detection: symptoms typically become evident only after the pathogen has colonized internal stem tissues, by which point control options are limited and economic losses are large [4].

Cite this article as: Indriani, S., Pancoro, A., Isdaryanti, Poleuleng, A. B., Ilmiah, S. N., Handayani, F. "GC–MS-Based Untargeted Metabolic Profiling of Oil Palm Stems Associated with *Ganoderma boninense* Infection", Periodica Polytechnica Chemical Engineering, 2026. https://doi.org/10.3311/PPch.44836

A recent work has therefore emphasized the use of molecular and biochemical approaches to better understand host–pathogen interactions and metabolic changes associated with infection [5]. Metabolomics, which provides a comprehensive view of small molecules in biological systems, offers a useful approach for examining changes in the biochemical phenotype of plants exposed to biotic stress. This approach has been applied to several plant–pathogen systems to characterize infection-associated metabolic changes and to identify metabolites that may warrant further investigation [6].

Gas chromatography–mass spectrometry (GC–MS) is widely used for metabolite profiling because it provides chromatographic separation together with mass spectral information for compound characterization [7]. The approach is particularly useful for detecting volatile and semi-volatile compounds and has been applied to the analysis of plant metabolites under biotic and abiotic stress conditions [8]. Its application to oil palm therefore provides an opportunity to examine changes in GC–MS-detectable metabolic features associated with *G. boninense* infection.

In oil palm, untargeted GC–MS studies have begun to characterize metabolic alterations associated with *G. boninense* infection, particularly in root tissues, where changes in organic acids, amino acids, and other metabolites have been reported [9]. Complementary studies using nuclear magnetic resonance (NMR) and liquid chromatography–mass spectrometry (LC–MS) approaches have further shown that the oil palm–*Ganoderma* interaction involves changes in several classes of metabolites, including compounds associated with phenolic metabolism, sterol composition, cell-wall modification, and oxidative stress responses [10, 11]. However, metabolic responses can vary according to tissue type and analytical platform. Although stem tissue is directly affected during BSR development, its metabolic response across different levels of disease severity has not been extensively characterized using untargeted GC–MS. It therefore remains unclear whether GC–MS-detectable features in infected stems follow metabolic patterns previously reported in other oil palm tissues or whether additional candidate features can be identified when samples are compared according to disease severity.

G. boninense is a lignocellulose-degrading white-rot fungus that produces oxidative and hydrolytic enzymes involved in the degradation of lignin and polysaccharides [12, 13]. Such activities can alter host tissue integrity and may influence carbon allocation and secondary metabolism during disease development. Characterizing metabolic changes in infected stem tissue may therefore provide information on the biochemical response associated with disease progression.

In light of these considerations, this study used an untargeted GC–MS metabolomics approach to characterize metabolic variation in oil palm stem tissue associated with *G. boninense* infection. Specifically, we aimed to:

1. characterize metabolic differences among healthy, low, moderate, and high infection categories;
2. identify metabolic features contributing to the observed differences;
3. prioritize candidate metabolites associated with disease severity for further investigation.

By focusing on stem tissue, this study provides additional information on the metabolic response of oil palm to *G. boninense* infection and allows the observed features to be considered in relation to metabolic responses previously reported in other oil palm tissues.

2 Materials and methods

2.1 Sample collection and disease severity classification

Stem samples were collected from 15-year-old oil palm trees at approximately 1.5 m above the ground at the Letawa oil palm plantation, Central Sulawesi, Indonesia. Stem sections measuring approximately 8 × 7 cm were collected from trees showing different field-observed levels of infection. Based on the physical characteristics of the trees and information provided by an oil palm specialist at the plantation, the samples were classified into four categories: healthy (Healthy), low infection (Low), moderate infection (Moderate), and high infection (High). A total of 12 stem samples were collected, with three biological samples representing each category ($n = 3$ per category), where n denotes the number of biological samples per infection category. No independent molecular, microbiological, or histological confirmation of *Ganoderma boninense* infection was performed. Therefore, the infection categories in this study represent field-based classifications rather than independently confirmed pathogen loads [10, 14].

2.2 Preparation and extraction of samples

Stem samples were immediately frozen and stored at −80 °C prior to extraction. The tissues were ground under liquid nitrogen, and 0.1 g of the resulting material was transferred into a 15-mL tube. The samples were lyophilized and extracted with 5 mL high-performance liquid chromatography (HPLC)-grade methanol (Merck, Germany). The mixtures were vortexed for 1 min and sonicated for

30 min under cold conditions. The samples were centrifuged at 4,000 rpm for 15 min at 4 °C, and the resulting supernatants were collected and transferred to 1.5-mL GC–MS vials for subsequent analysis. The instruments used for sample preparation were as follows: a refrigerated centrifuge (5810 R, Eppendorf, Germany), an ultrasonic bath sonicator (Branson 5800, Branson Ultrasonics, USA), and a laboratory freeze dryer (FreeZone, Labconco, USA). This sample preparation procedure was based on previously reported metabolomics workflows in plants, including oil palm tissues [15–18].

2.3 Sample analysis using gas chromatography–mass spectrometry

Methanolic extracts were analyzed using an Agilent 6890N gas chromatograph coupled with an Agilent 5973 mass selective detector (Agilent Technologies, USA) and equipped with a J&W DB-5 capillary column (Agilent Technologies, USA; 30 m × 0.25 mm internal diameter, 0.25 μm film thickness). Helium was used as the carrier gas at 0.7 mL min^{-1}. The oven temperature was held at 180 °C for 5 min, increased to 260 °C at 3 °C min^{-1}, then to 280 °C and held for 5 min. The injector and detector temperatures were 280 °C and 290 °C, respectively. Mass spectra were acquired by electron ionization (EI) at 70 eV in full-scan mode (mass-to-charge ratio (*m/z*) 30–600), with ion source and quadrupole temperatures of 290 °C and 100 °C, respectively, and a 7-min solvent delay. A non-derivatized approach was used, in which metabolites were directly extracted with methanol and injected into the GC–MS system, enabling analysis of extractable, volatile, and semi-volatile compounds.

2.4 Metabolomic data analysis using MetaboAnalyst

2.4.1 Data processing

The GC–MS output files were converted into comma-separated values (CSV) format containing mass-to-charge ratio, retention time, and peak intensity information for each sample. The datasets were organized according to the four field-observed infection categories (Healthy, Low, Moderate, and High), with three biological samples represented in each category, and were combined into a single dataset for analysis in MetaboAnalyst [19]. Following data upload, the dataset structure and integrity were checked within the platform. Feature filtering was performed to reduce the contribution of features with insufficient data coverage across the samples. The retained features were subsequently subjected to limit-of-detection (LOD) imputation for missing values, followed by log2 transformation and Pareto scaling. These preprocessing steps were applied before multivariate statistical analyses to improve comparability among samples and reduce the influence of differences in feature abundance [20, 21].

2.4.2 Principal component analysis

Principal component analysis (PCA) was performed in MetaboAnalyst as an unsupervised method to examine the overall variation in the processed GC–MS feature dataset and the distribution of samples across the four field-observed infection categories. The first two principal components (PC1 and PC2) were used to generate two-dimensional score plots for visualizing sample distribution and potential clustering patterns. Loading information was examined to identify features contributing to the variation represented by the principal components. PCA was used primarily to explore the overall structure of the dataset and to assess whether samples from different infection categories showed distinguishable metabolic patterns [20, 21].

2.4.3 Partial least square-discriminant analysis

Partial least squares-discriminant analysis (PLS-DA) was performed in MetaboAnalyst as a supervised multivariate approach to examine whether the processed GC–MS features could distinguish the four field-observed infection categories. Two-dimensional and three-dimensional score plots were generated to visualize the distribution of samples in the latent-variable space. Variable importance in projection (VIP) scores were used to identify features that contributed most to the fitted model, with features showing higher VIP values prioritized for further examination. Model performance was assessed using cross-validation and permutation testing to evaluate the stability of the observed class separation and the possibility of overfitting. Because of the limited number of biological samples in each category, the PLS-DA results were interpreted as exploratory rather than as evidence of a validated classification model [20, 21]. Model performance was assessed using cross-validation and permutation testing to evaluate the stability of the observed class separation and the possibility of overfitting. R^2 represents the proportion of variation explained by the PLS-DA model, whereas Q^2 represents its predictive performance estimated by cross-validation.

2.4.4 Univariate statistical analysis

Univariate statistical analysis was performed to complement the multivariate analyses and to evaluate differences in individual GC–MS features among the four field-observed infection categories. One-way analysis of variance

(ANOVA) was applied to the retained features, and the resulting *p*-values were adjusted using the false discovery rate (FDR) procedure to account for multiple testing. A nominal significance level of $p < 0.05$ was used for the initial assessment, where p denotes the probability value obtained from the statistical test. FDR-adjusted *q*-values < 0.05, where *q* denotes the FDR-adjusted *p*-value, were considered statistically significant.

3 Results and discussion

3.1 Data filtering

Data filtering was performed to remove low-information features and reduce analytical noise in the untargeted metabolomics dataset [22]. Missing values, which may result from signals below the detection limit, were handled using the selected imputation approach in MetaboAnalyst to minimize potential bias in downstream analyses [23, 24]. The relatively low number of GC–MS features may reflect the methanolic extraction, GC–MS conditions, and feature filtering procedures, as well as the limited number of field-collected samples. Thus, the retained features represent detectable and reproducible metabolic variation within this dataset rather than the complete oil palm stem metabolome.

The initial GC–MS dataset comprised 12 samples and 15 features, with 91 missing values (50.6%), as summarized in Table 1. Data filtering was performed in MetaboAnalyst using an interquartile range (IQR)-based low-variance filter, with the lowest 5% of features removed. One feature (GC_RT_41_205) was excluded, resulting in 14 retained features for downstream analysis. Missing values in the retained features were subsequently imputed prior to data transformation and scaling [25]. Feature codes beginning with "GC_RT" refer to GC–MS features defined by their retention time in minutes. For example, GC_RT_23_887 denotes a feature detected at a retention time of 23.887 min.

Table 1 Feature filtering based on data coverage

Feature	Missing samples ($n = 12$)	Missing (%)	Decision
GC_RT_15_060	9	75.0	Retained
GC_RT_18_223	8	66.7	Retained
GC_RT_23_887	9	75.0	Retained
GC_RT_24_730	4	33.3	Retained
GC_RT_26_945	8	66.7	Retained
GC_RT_29_858	7	58.3	Retained
GC_RT_30_633	6	50.0	Retained
GC_RT_35_267	9	75.0	Retained
GC_RT_36_008	1	8.3	Retained
GC_RT_36_929	4	33.3	Retained
GC_RT_40_302	1	8.3	Retained
GC_RT_40_905	9	75.0	Retained
GC_RT_41_205	7	58.3	Removed
GC_RT_41_312	7	58.3	Retained
GC_RT_44_674	2	16.7	Retained

3.2 Data normalization

Missing values in the 14 retained features were imputed using the LOD method in MetaboAnalyst. The imputed data were subsequently log2-transformed to reduce skewness and the influence of high-intensity signals, followed by Pareto scaling to reduce the dominance of highly abundant features while preserving the overall data structure. The resulting dataset was used for subsequent PCA and PLS-DA analyses [26].

As shown in Fig. 1, preprocessing reduced differences in signal magnitude and improved comparability among samples. Following LOD imputation, log2 transformation reduced the influence of highly skewed intensities, while Pareto scaling moderated the contribution of high-abundance features while retaining substantial data variation. The processed dataset was therefore considered suitable for subsequent multivariate analyses [27].

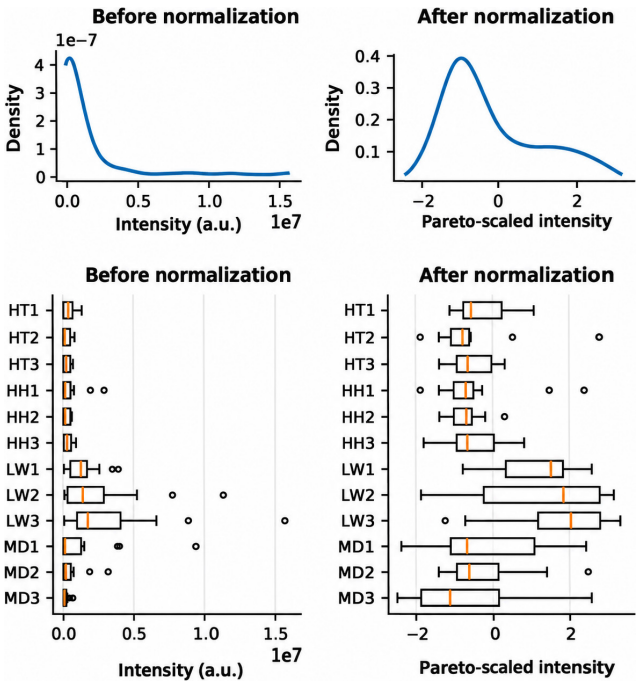


Fig. 1 GC–MS feature distributions before and after LOD imputation, log2 transformation, and Pareto scaling, shown as kernel density plots and boxplots

The boxplots showed substantial differences in signal magnitude and variance before preprocessing, with several extreme values influencing the data structure. Following feature filtering, the 14 retained features underwent LOD imputation, log2 transformation, and Pareto scaling. These steps reduced skewness and the influence of extreme signal intensities, resulting in more comparable distributions across samples while preserving relevant variation. The processed dataset was subsequently used for PCA and PLS-DA [28].

The retained GC–MS features were putatively annotated as fatty-acid-related compounds, alkane hydrocarbons, and other library-matched compounds (Table 2). Fatty acids are important components of cellular membranes and precursors of lipid-derived signaling molecules, including oxylipins involved in plant defense responses [29, 30]. Several features were annotated as methyl esters of decanoic, dodecanoic, tetradecanoic, hexadecanoic, and octadecenoic acids, together with pentadecanoic and octadecenoic acids. These annotations suggest that lipid-associated metabolism may contribute to the metabolic variation observed among the sampled infection categories. However, because the annotations were based on mass-spectral library matching without authentic-standard confirmation, they should be considered putative rather than confirmed metabolites. Similar alterations in lipid-associated metabolites have been reported in the oil palm–*Ganoderma* pathosystem, supporting a potential role of lipid metabolism in host responses [31]. Nevertheless, the present data do not establish a direct causal relationship between individual fatty-acid-related features and *G. boninense* infection.

3.3 Principal component analysis

PCA was performed as an unsupervised multivariate analysis to evaluate the overall variation and distribution of the 14 retained GC–MS features across the four field-observed infection categories. By reducing correlated variables into principal components, PCA facilitates visualization of major metabolic patterns and sample similarities or differences [20, 21, 32–34].

As shown in Fig. 2, PC1 and PC2 explained 54.6% and 18.4% of the total variance, respectively (73.0% combined). Low-infection samples tended to cluster on the negative side of PC1, whereas Healthy, Moderate-, and High-infection samples were mainly distributed on the positive side. However, substantial overlap among the latter three groups indicated that their metabolic profiles were not clearly separated by the first two principal components.

The Low-infection group showed the clearest displacement from the other categories, with all three samples located on the negative side of PC1, whereas Healthy, Moderate-, and High-infection samples showed greater overlap. Variation among Moderate- and High-infection samples further indicated within-category heterogeneity. Overall, the PCA suggested metabolic variation associated with field-observed infection categories but did not provide complete separation among groups. Given the field-based classification and small number of biological samples (n = 3 per category), these patterns should be interpreted as exploratory rather than as definitive evidence of disease-stage discrimination.

The PCA pattern was broadly consistent with previous metabolomics studies of the oil palm–*Ganoderma boninense* pathosystem [10, 35]. However, differences in

Table 2 Putative compound annotations of the retained GC–MS features

Feature	Retention time (min)	Putative compound annotation	Chemical class
GC_RT_15_060	15.060	5-(Hydroxymethyl)-2-furancarboxaldehyde (HMF)	Furan derivative
GC_RT_18_223	18.223	Decanoic acid, methyl ester (methyl caprate)	Fatty acid ester
GC_RT_23_887	23.887	Heptadecane / Hexadecane	Alkane hydrocarbon
GC_RT_24_730	24.730	Dodecanoic acid, methyl ester (methyl laurate)	Fatty acid ester
GC_RT_26_945	26.945	Hexadecane / Heneicosane	Alkane hydrocarbon
GC_RT_29_858	29.858	Eicosane / Heptadecane	Alkane hydrocarbon
GC_RT_30_633	30.633	Methyl tetradecanoate (methyl myristate)	Fatty acid ester
GC_RT_35_267	35.267	Nonadecane / Pentacosane	Alkane hydrocarbon
GC_RT_36_008	36.008	Hexadecanoic acid, methyl ester (methyl palmitate)	Fatty acid ester
GC_RT_36_929	36.929	Pentadecanoic acid	Fatty acid
GC_RT_40_302	40.302	9-Octadecenoic acid (Z)-, methyl ester (methyl oleate)	Fatty acid ester
GC_RT_40_905	40.905	Octadecanoic acid, methyl ester	Fatty acid ester
GC_RT_41_312	41.312	Octadec-9-enoic acid	Unsaturated fatty acid
GC_RT_44_674	44.674	9-Octadecenoic acid, 12-hydroxy-, methyl ester	Hydroxy fatty acid ester

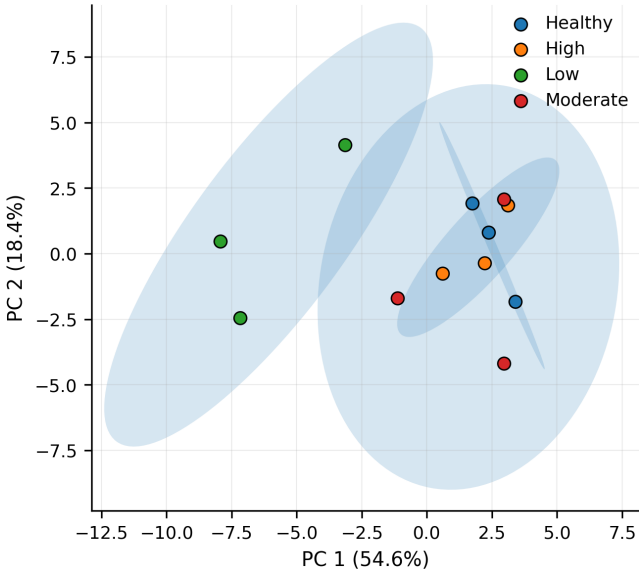


Fig. 2 PCA score plot of oil palm stem samples based on 14 retained GC–MS features across four field-observed infection categories

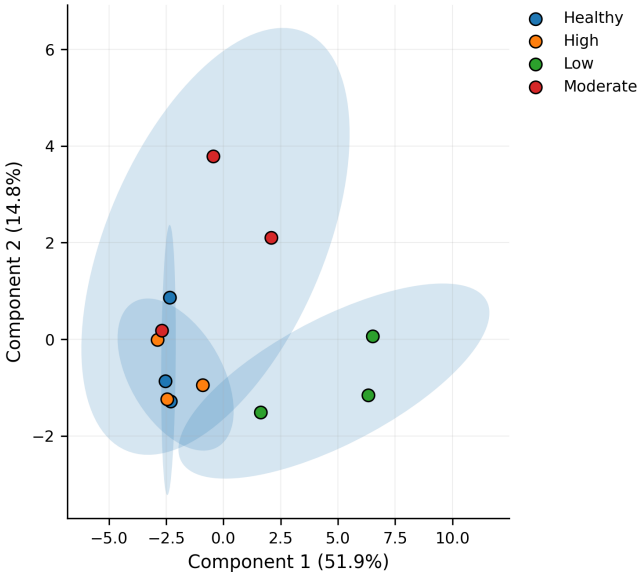


Fig. 3 PLS-DA score plot of oil palm stem samples based on 14 retained GC–MS features across four field-observed infection categories

analytical platforms, tissue types, and retained features limited direct comparison. The Low-infection samples showed the clearest displacement along PC1, while overlap among the other categories indicated that metabolic variation did not follow a simple linear pattern of field-observed disease severity. Further analyses are needed to identify consistently associated features.

3.4 Partial least squares-discriminant analysis

PLS-DA was subsequently performed as a supervised multivariate approach to evaluate discrimination among the four field-observed infection categories by incorporating class information into latent component construction [33].

As shown in Fig. 3, the first and second PLS-DA components explained 51.9% and 14.8% of the modeled variation, respectively, corresponding to 66.7% of the total variation represented by the first two components. The score distribution showed a clearer group-related pattern than that observed in the PCA. The Low-infection samples were positioned predominantly on the positive side of Component 1, whereas the Moderate-infection samples were distributed mainly toward the upper region of the score plot. The Healthy and High-infection samples were located relatively close to each other and showed substantial overlap. Several Moderate-infection samples also overlapped with the Healthy and High-infection groups.

The displacement of the Low-infection samples along Component 1 suggests that some retained GC–MS features contributed to group-related metabolic variation, whereas overlap among Healthy, Moderate-, and High-infection samples indicated limited discrimination. Thus, the PLS-DA pattern should be interpreted as exploratory rather than definitive evidence of disease-stage classification. This finding is broadly consistent with previous PLS-DA studies of the oil palm–*Ganoderma boninense* pathosystem [10, 35], although differences in analytical platform, tissue type, and feature number limit direct comparison.

Because PLS-DA is supervised, apparent group separation may be exaggerated in small datasets. Cross-validation and permutation testing were therefore used to assess model robustness [10, 35]. Accordingly, the PLS-DA pattern was interpreted as exploratory group-related metabolic variation rather than definitive classification.

3.5 Partial least squares-discriminant analysis model validation

Five-fold cross-validation was performed using one to three latent components to assess PLS-DA model robustness. Classification accuracy remained low (0.42–0.45), while R^2 increased from 0.20 to 0.48 and 0.67 with increasing components. However, Q^2 values remained negative, indicating limited predictive performance under cross-validation. Permutation testing further showed no significant evidence of model performance beyond chance ($p = 0.121$) (Fig. 4 (a)).

Permutation testing with 1,000 permutations yielded $p = 0.121$, indicating no significant evidence that the observed PLS-DA discrimination exceeded that obtained from permuted class assignments (Fig. 4 (b)). Together with the negative Q^2 values, these results indicate limited model robustness. The PLS-DA separation was therefore interpreted as an exploratory metabolic pattern rather than a validated

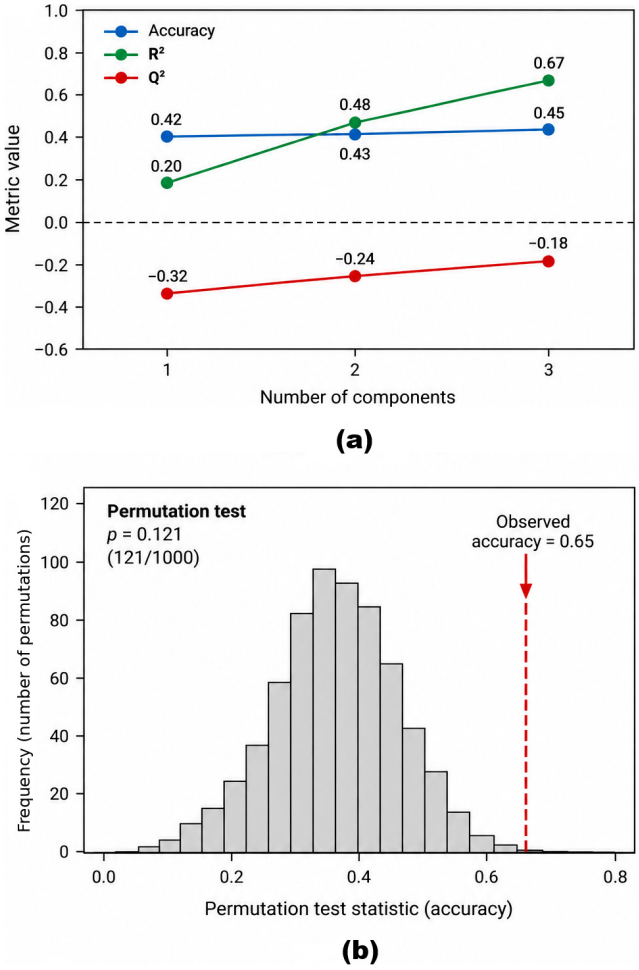


Fig. 4 PLS-DA model validation based on: (a) five-fold cross-validation; (b) 1,000-permutation testing

classification model. The limited performance may partly reflect the small number of biological samples ($n = 3$ per category); consequently, PLS-DA was used primarily to prioritize features for subsequent VIP and univariate analyses.

3.6 Variable importance in projection analysis

VIP scores were used to assess the relative contribution of individual GC–MS features to the PLS-DA model. Features with VIP >1 were considered a preliminary criterion for prioritization in subsequent analyses, rather than evidence of statistical significance or confirmed biomarker status [34].

As shown in Fig. 5, seven of the 14 retained features had VIP values greater than 1. The highest VIP score was observed for GC_RT_26_945 (VIP = 1.43), followed by GC_RT_18_223 (VIP = 1.39), GC_RT_40_905 (VIP = 1.21), GC_RT_29_858 (VIP = 1.21), GC_RT_35_267 (VIP = 1.17), GC_RT_30_633 (VIP = 1.13), and GC_RT_36_929 (VIP = 1.10). These features therefore made relatively

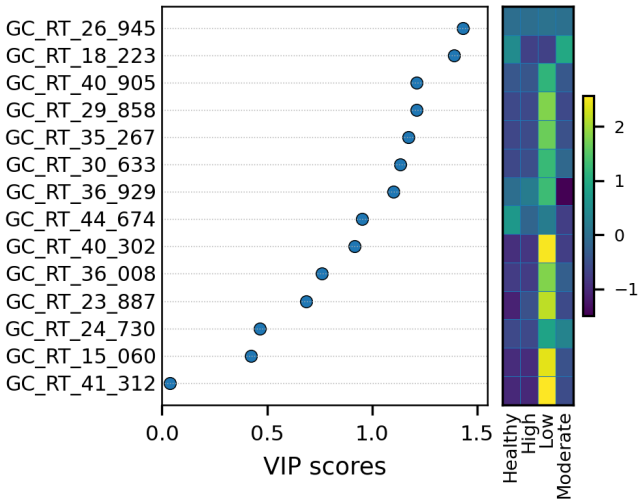


Fig. 5 Variable importance in projection (VIP) scores of the 14 retained GC–MS features derived from the PLS-DA model

greater contributions to the class-related variation captured by the PLS-DA model than the other retained features.

VIP ranking was not fully consistent with univariate results. GC_RT_26_945 and GC_RT_18_223 had high VIP scores and nominally significant ANOVA results ($p = 0.025$), while GC_RT_29_858 was also significant at $p = 0.042$; however, none remained significant after FDR correction. Conversely, GC_RT_23_887 had the lowest nominal ANOVA p-value ($p = 0.013$) but a VIP < 1 (0.69), indicating that VIP and univariate analyses capture different aspects of metabolic variation. Given the limited PLS-DA robustness, the seven features with VIP > 1 were considered priority features for further investigation rather than confirmed biomarkers.

3.7 Univariate statistical analysis

One-way ANOVA was performed to assess differences in individual GC–MS feature abundances among the four field-observed infection categories (Healthy, Low, Moderate, and High), with p-values adjusted using FDR (Fig. 6). Five features showed nominal significance ($p < 0.05$): GC_RT_23_887 ($p = 0.013$), GC_RT_18_223 and GC_RT_26_945 ($p = 0.025$), GC_RT_29_858 ($p = 0.042$), and GC_RT_44_674 ($p = 0.049$). However, none remained significant after FDR correction ($q = 0.119$–0.138), indicating that these differences should be considered exploratory rather than statistically confirmed.

The ANOVA results in Fig. 6 also showed that not all features contributing to the PLS-DA model exhibited strong univariate differences. For example, GC_RT_26_945 and GC_RT_18_223 had relatively high VIP scores (>1) and

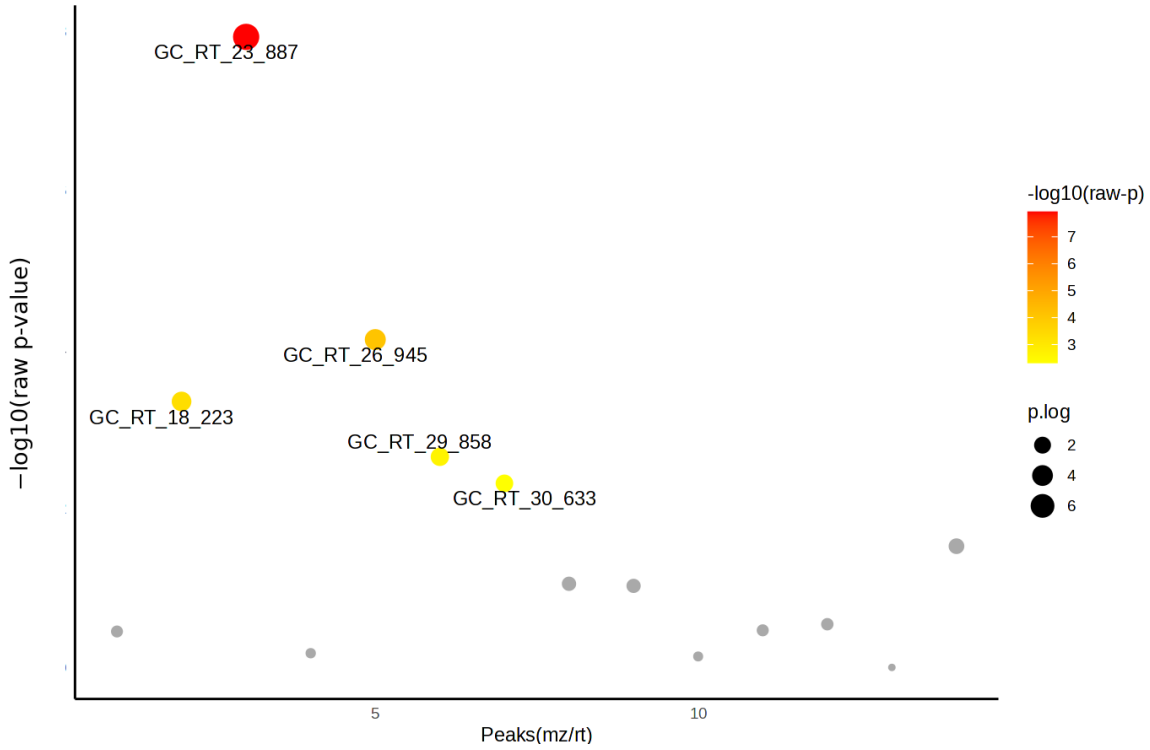


Fig. 6 ANOVA results for the 14 retained GC–MS features across the four field-observed infection categories

nominal ANOVA significance, whereas GC_RT_36_929 had a VIP score above 1 but showed no evidence of a univariate difference ($p = 0.809$). Conversely, GC_RT_23_887 had the lowest ANOVA p-value ($p = 0.013$) but a VIP score below 1. This difference between multivariate and univariate rankings indicates that the contribution of a feature to the overall multivariate pattern does not necessarily correspond to its univariate statistical significance.

4 Conclusion

Untargeted GC–MS metabolomics revealed metabolic variation among oil palm stem samples representing different field-observed infection categories associated with *Ganoderma boninense*. After data processing and filtering, 14 GC–MS features were retained for multivariate and univariate analyses. PCA and PLS–DA revealed group-related metabolic patterns, while VIP analysis highlighted several fatty acid-related features, including methyl decanoate, methyl myristate, methyl oleate, methyl stearate, and methyl ricinoleate, as candidate features associated with disease severity. However, permutation testing did not support a validated PLS–DA classification model, and none of the features remained significant after FDR correction. Therefore, these features should be regarded as preliminary candidate metabolites rather than confirmed biomarkers. Further validation using larger, independent sample sets and targeted quantitative analyses is required to establish their biological relevance and potential diagnostic value for basal stem rot in oil palm.

Acknowledgement

The authors gratefully acknowledge the financial support provided for the publication of this article by the Ministry of Higher Education, Science, and Technology, Directorate General of Research and Development, Republic of Indonesia. This support was instrumental in enabling the dissemination of our research findings.

References

[1] Alhaji, A. M., Almeida, E. S., Carneiro, C. R., da Silva, C. A. S., Monteiro, S., Coimbra, J. S. d. R. "Palm Oil (*Elaeis guineensis*): A Journey through Sustainability, Processing, and Utilization", Foods, 13(17), 2814, 2024. https://doi.org/10.3390/foods13172814

[2] Mweta, N., Obeng, A. S., Ansah, J. W. "Socio-economic benefits and challenges confronting oil palm production among indigenous rural farmers in Karonga district, Malawi", Frontiers in Sustainable Food Systems, 9, 1473991, 2025. https://doi.org/10.3389/fsufs.2025.1473991

[3] Khoo, Y. W., Chong, K. P. "*Ganoderma boninense*: general characteristics of pathogenicity and methods of control", Frontiers in Plant Science, 14, 1156869, 2023. https://doi.org/10.3389/fpls.2023.1156869

[4] Ahmadi, P., Muharam, F. M., Ahmad, K., Mansor, S., Seman, I. A. "Early Detection of Ganoderma Basal Stem Rot of Oil Palms using Artificial Neural Network Spectral Analysis", Plant Disease, 101(6), pp. 1009–1016, 2017. https://doi.org/10.1094/PDIS-12-16-1699-RE

[5] Bharudin, I., Ab Wahab, A. F. F., Abd Samad, M. A., Xin Yie, N., Zairun, M. A., Abu Bakar, F. D., Abdul Murad, A. M. "Review Update on the Life Cycle, Plant–Microbe Interaction, Genomics, Detection and Control Strategies of the Oil Palm Pathogen *Ganoderma boninense*", Biology, 11(2), 251, 2022. https://doi.org/10.3390/biology11020251

[6] Li, B., Fu, Y., Xi, H., Liu, S., Zhao, W., Li, P., Fan, W., Wang, D., Sun, S. "Untargeted Metabolomics Using UHPLC-HRMS Reveals Metabolic Changes of Fresh-Cut Potato during Browning Process", Molecules, 28(8), 3375, 2023. https://doi.org/10.3390/molecules28083375

[7] Frolova, N., Bilova, T., Silinskaia, S., Orlova, A., Gurina, A., Frolov, A. "Gas Chromatography–Mass Spectrometry (GC-MS) in the Plant Metabolomics Toolbox: GC-MS in Multi-Platform Metabolomics and Integrated Multi-Omics Research", International Journal of Molecular Sciences, 27(3), 1343, 2026. https://doi.org/10.3390/ijms27031343

[8] Frolova, N., Orlova, A., Popova, V., Bilova, T., Frolov, A. "GC-MS-based metabolomics – Part 1 Gas chromatography-mass spectrometry (GC-MS) and its place in the plant metabolomics toolbox", ChemRxiv, 2025. https://doi.org/10.26434/chemrxiv-2025-5kgvt

[9] Isha, A., Yusof, N. A., Shaari, K., Osman, R., Abdullah, S. N. A., Wong, M.-Y. "Metabolites identification of oil palm roots infected with *Ganoderma boninense* using GC–MS-based metabolomics", Arabian Journal of Chemistry, 13(7), pp. 6191–6200, 2020. https://doi.org/10.1016/j.arabjc.2020.05.026

[10] Pancoro, A., Karima, E., Apriyanto, A., Effendi, Y. "^{1}H NMR metabolomics analysis of oil palm stem tissue infected by *Ganoderma boninense* based on field severity Indices", Scientific Reports, 12(1), 21087, 2022. https://doi.org/10.1038/s41598-022-25450-5

[11] Baharum, S. N., Ahmad, M. F., Ajeng, A. A., Abdullah, R. "Metabolites profiling of *Ganoderma*-infected oil palms rachis grown on tropical soils reveals choline phosphate and 2-oxoglutaramate as potential biomarkers in the disease detection", Physiological and Molecular Plant Pathology, 125, 102001, 2023. https://doi.org/10.1016/j.pmpp.2023.102001

[12] Karunarathna, S. C., Patabendige, N. M., Lu, W., Asad, S., Hapuarachchi, K. K. "An In-Depth Study of Phytopathogenic *Ganoderma*: Pathogenicity, Advanced Detection Techniques, Control Strategies, and Sustainable Management", Journal of Fungi, 10(6), 414, 2024. https://doi.org/10.3390/jof10060414

[13] Martín-Gómez, A., Rodríguez-Hernández, P., Cardador, M. J., Vega-Márquez, B., Rodríguez-Estévez, V., Arce, L. "Guidelines to build PLS-DA chemometric classification models using a GC-IMS method: Dry-cured ham as a case of study", Talanta Open, 7, 100175, 2023. https://doi.org/10.1016/j.talo.2022.100175

[14] Husin, N. A., Khairunniza-Bejo, S., Abdullah, A. F., Kassim, M. S. M., Ahmad, D., Aziz, M. H. A. "Classification of Basal Stem Rot Disease in Oil Palm Plantations Using Terrestrial Laser Scanning Data and Machine Learning", Agronomy, 10(11), 1624, 2020. https://doi.org/10.3390/agronomy10111624

[15] Indriani, S., Isdaryanti, I., Agustia, M., Poleuleng, A. B., Syahra, N. J., Prastiyo, Y. B. "Analisis GC-MS (Gass Cromatography-Mass Spectrometry) Terhadap Batang Kelapa Sawit (*Elaeis guineesis* Jaq.)" (GC-MS (Gass Cromatography-Mass Spectrometry) Analysis of Palm Oil Stem (*Elaeis guineesis* Jaq.)), Agroplantae: Jurnal Ilmiah Terapan Budidaya Dan Pengelolaan Tanaman Pertanian Dan Perkebunan, 12(2), pp. 147–155, 2023. (in Indonesian) https://doi.org/10.51978/agro.v12i2.527

[16] Vargas, L. H. G., Neto, J. C. R., de Aquino Ribeiro, J. A., Ricci-Silva, M. E., Souza, M. T., Rodrigues, C. M., de Oliveira, A. E., Abdelnur, P. V. "Metabolomics analysis of oil palm (*Elaeis guineensis*) leaf: evaluation of sample preparation steps using UHPLC–MS/MS", Metabolomics, 12(10), 153, 2016. https://doi.org/10.1007/s11306-016-1100-z

[17] Xue, T., Liu, S., Liu, J., Yuan, Y. "Metabolomics based on GC-MS revealed hub metabolites of pecan seeds germinating at different temperatures", BMC Plant Biology, 23(1), 192, 2023. https://doi.org/10.1186/s12870-023-04209-8

[18] Nusaibah, S. A., Siti Nor Akmar, A., Idris, A. S., Sariah, M., Mohamad Pauzi, Z. "Involvement of metabolites in early defense mechanism of oil palm (*Elaeis guineensis* Jacq.) against *Ganoderma* disease", Plant Physiology and Biochemistry, 109, pp. 156–165, 2016. https://doi.org/10.1016/j.plaphy.2016.09.014

[19] Xia Lab @ McGill "MetaboAnalyst, (6.0)", [computer program] Available at: https://www.metaboanalyst.ca/ [Accessed: 21 May 2026]

[20] Chong, J., Wishart, D. S., Xia, J. "Using MetaboAnalyst 4.0 for Comprehensive and Integrative Metabolomics Data Analysis", Current Protocols in Bioinformatics, 68(1), e86, 2019. https://doi.org/10.1002/cpbi.86

[21] Pang, Z., Lu, Y., Zhou, G., Hui, F., Xu, L., …, Xia, J. "MetaboAnalyst 6.0: towards a unified platform for metabolomics data processing, analysis and interpretation", Nucleic Acids Research, 52(W1), pp. W398–W406, 2024. https://doi.org/10.1093/nar/gkae253

[22] Schiffman, C., Petrick, L., Perttula, K., Yano, Y., Carlsson, H., Whitehead, T., Metayer, C., Hayes, J., Rappaport, S., Dudoit, S. "Filtering procedures for untargeted LC-MS metabolomics data", BMC Bioinformatics, 20(1), 334, 2019. https://doi.org/10.1186/s12859-019-2871-9

[23] Playdon, M. C., Joshi, A. D., Tabung, F. K., Cheng, S., Henglin, M., …, Zeleznik, O. A. "Metabolomics Analytics Workflow for Epidemiological Research: Perspectives from the Consortium of Metabolomics Studies (COMETS)", Metabolites, 9(7), 145, 2019. https://doi.org/10.3390/metabo9070145

[24] Pang, Z., Xia, J. "Functional Analysis of Global Metabolomics", MetaboAnalyst, 23 July 2023. [online] Available at: https://dev.metaboanalyst.ca/resources/vignettes/Functional_Analysis_global_metabolomics.html [Accessed: 01 December 2025]

[25] Magar, V., Ruikar, D., Bhoite, S., Mente, R. "Innovative Inter Quartile Range-based Outlier Detection and Removal Technique for Teaching Staff Performance Feedback Analysis", Journal of Engineering Education Transformations, 37(3), pp. 176–184, 2025. https://doi.org/10.16920/jeet/2024/v37i3/24013

[26] Li, B., Tang, J., Yang, Q., Li, S., Cui, X., Li, Y., Chen, Y., Xue, W., Li, X., Zhu, F. "NOREVA: normalization and evaluation of MS-based metabolomics data", Nucleic Acids Research, 45(W1), pp. W162–W170, 2017. https://doi.org/10.1093/nar/gkx449

[27] Tseng, C. Y., Salguero, J. A., Breidenbach, J. D., Solomon, E., Sanders, C. K., …, Glaros, T. G. "Evaluation of normalization strategies for mass spectrometry-based multi-omics datasets", Metabolomics, 21(4), 98, 2025. https://doi.org/10.1007/s11306-025-02297-1

[28] Sun, J., Xia, Y. "Pretreating and normalizing metabolomics data for statistical analysis", Genes & Diseases, 11(3), 100979, 2024. https://doi.org/10.1016/j.gendis.2023.04.018

[29] Toncan, F., Raj, R. R., Lee, M.-J. "Dynamics of Fatty Acid Composition in Lipids and Their Distinct Roles in Cardiometabolic Health", Biomolecules, 15(5), 696, 2025. https://doi.org/10.3390/biom15050696

[30] Seth, T., Asija, S., Umar, S., Gupta, R. "The intricate role of lipids in orchestrating plant defense responses", Plant Science, 338, 111904, 2024. https://doi.org/10.1016/j.plantsci.2023.111904

[31] Kuźniak, E., Gajewska, E. "Lipids and Lipid-Mediated Signaling in Plant–Pathogen Interactions", International Journal of Molecular Sciences, 25(13), 7255, 2024. https://doi.org/10.3390/ijms25137255

[32] Curtasu, M. V., Levinsen, J. U. G., Bruhn, A., Nielsen, M. O., Nørskov, N. P. "Metabolomic Insights into the Phytochemical Profiles and Seasonal Shifts of *Fucus serratus* and *F. vesiculosus* Harvested in Danish Coastal Waters (Aarhus Bay)—An Untargeted High-Resolution Mass-Spectrometry Approach", Marine Drugs, 23(11), 417, 2025. https://doi.org/10.3390/md23110417

[33] Anastasiou, I. A., Kounatidis, D., Honka, M.-J., Vallianou, N. G., Rebelos, E., Karamanolis, N. N., Dalamaga, M., Pantos, C., Mourouzis, I. "Metabolomic Alterations in Patients with Obesity and the Impact of Metabolic Bariatric Surgery: Insights for Future Research", Metabolites, 15(7), 434, 2025. https://doi.org/10.3390/metabo15070434

[34] Stocchero, M., Locci, E., d'Aloja, E., Nioi, M., Baraldi, E., Giordano, G. "PLS2 in Metabolomics", Metabolites, 9(3), 51, 2019. https://doi.org/10.3390/metabo9030051

[35] Nugroho, S., Rahmadi, H. Y., Simamora, A. N., Purba, A. R. "^{1}H NMR metabolomic profiling of resistant and susceptible oil palm root tissues in response to *Ganoderma boninense* at the nursery stage", Scientific Reports, 15(1), 16784, 2025. https://doi.org/10.1038/s41598-025-01691-y